Dust measurements in tokamaks (invited)[a)]

D. L. Rudakov,[1] J. H. Yu,[1] J. A. Boedo,[1] E. M. Hollmann,[1] S. I. Krasheninnikov,[1] R. A. Moyer,[1] S. H. Muller,[1] A. Yu. Pigarov,[1] M. Rosenberg,[1] R. D. Smirnov,[1] W. P. West,[2] R. L. Boivin,[2] B. D. Bray,[2] N. H. Brooks,[2] A. W. Hyatt,[2] C. P. C. Wong,[2] A. L. Roquemore,[3] C. H. Skinner,[3] W. M. Solomon,[3] S. Ratynskaia,[4] M. E. Fenstermacher,[5] M. Groth,[5] C. J. Lasnier,[5] A. G. McLean,[6] and P. C. Stangeby[6]
[1]*University of California, San Diego, California 92093, USA*
[2]*General Atomics, P.O. Box 85608, San Diego, California 92186-5608, USA*
[3]*Princeton Plasma Physics Laboratory, Princeton, New Jersey 08543, USA*
[4]*Space and Plasma Physics, EE, Royal Institute of Technology, SE-10044 Stockholm, Sweden*
[5]*Lawrence Livermore National Laboratory, Livermore, California 94550, USA*
[6]*University of Toronto Institute for Aerospace Studies, Toronto, Ontario M3H 5T6, Canada*

(Presented 14 May 2008; received 9 May 2008; accepted 21 July 2008; published online 31 October 2008)

Dust production and accumulation present potential safety and operational issues for the ITER. Dust diagnostics can be divided into two groups: diagnostics of dust on surfaces and diagnostics of dust in plasma. Diagnostics from both groups are employed in contemporary tokamaks; new diagnostics suitable for ITER are also being developed and tested. Dust accumulation in ITER is likely to occur in hidden areas, e.g., between tiles and under divertor baffles. A novel electrostatic dust detector for monitoring dust in these regions has been developed and tested at PPPL. In the DIII-D tokamak dust diagnostics include Mie scattering from Nd:YAG lasers, visible imaging, and spectroscopy. Laser scattering is able to resolve particles between 0.16 and 1.6 μm in diameter; using these data the total dust content in the edge plasmas and trends in the dust production rates within this size range have been established. Individual dust particles are observed by visible imaging using fast framing cameras, detecting dust particles of a few microns in diameter and larger. Dust velocities and trajectories can be determined in two-dimension with a single camera or three-dimension using multiple cameras, but determination of particle size is challenging. In order to calibrate diagnostics and benchmark dust dynamics modeling, precharacterized carbon dust has been injected into the lower divertor of DIII-D. Injected dust is seen by cameras, and spectroscopic diagnostics observe an increase in carbon line (CI, CII, C_2 dimer) and thermal continuum emissions from the injected dust. The latter observation can be used in the design of novel dust survey diagnostics. [DOI: 10.1063/1.2969422]

I. INTRODUCTION

Dust is commonly found in magnetic fusion devices.[1–8] In contemporary machines dust is generally of little concern from an operational or safety standpoint. However, dust generation in the next-step devices is expected to increase by several orders of magnitude due to the increased duty cycle and higher magnitude of particle and power fluxes deposited on the plasma facing components (PFCs). Dust production and accumulation present potential safety and operational issues for the ITER by contributing to tritium inventory rise and leading to radiological and explosion hazards. The total in-vessel dust inventory in ITER will be limited to 1000 kg to ensure that environmental releases stay below the design limits in the case of the worst credible accident. A lower administrative limit of 670 kg has been proposed to take account of measurement uncertainties. The enhanced chemical activity of dust at high temperatures is more restrictive, since, in a case of in-vessel coolant leak, hot Be and C dust can react with steam/water causing hydrogen generation and (in a case of simultaneous air ingress) explosion hazard. Thus a limit of 11 kg for Be and 15 kg for C dust on hot surfaces is being considered. More projections of dust production and accumulation rates based on experience from existing tokamaks and disruption simulators are needed. In addition, dust penetration of the core plasma can cause undesirably high impurity concentration and degrade performance. Thus, studies of the dust transport and dynamics are also quite important.

Dust particulates found in tokamaks and other fusion devices range in size between ~10 nm and a few hundred micrometers.[1,3–8] Chemical composition of dust is determined mainly by the PFC materials, though dust particles may also contain plasma fuel elements (hydrogen isotopes) and radioactive elements generated by neutron bombardment of PFCs and dust. Dust production mechanisms in tokamaks with carbon-based PFCs include flaking of redeposited layers, brittle destruction of graphite, arcing, agglomeration from supersaturated vapor, and growth from hydrocarbon molecules.[6] Additionally, disruptions, large edge localized modes (ELMs) and other transient events result in increased dust production.[5,7,8]

Dust diagnostic techniques are not yet adequately devel-

[a)]Invited paper, published as part of the Proceedings of the 17th Topical Conference on High-Temperature Plasma Diagnostics, Albuquerque, New Mexico, May 2008.

oped to make quantitative predictions for the next-step devices; however, significant progress has been made in recent years. Reviews of dust measurements in fusion devices are available in Refs. 8–10. Here in Sec. II we will give a brief review of the dust diagnostic techniques currently employed in tokamaks and those proposed for the next-step devices. Then in Sec. III we will discuss dust diagnostics and dust measurements on the DIII-D tokamak and possible extension of those techniques for future devices.

II. DUST MEASUREMENTS IN EXISTING TOKAMAKS AND DIAGNOSTICS PROPOSED FOR NEXT-STEP DEVICES

Dust diagnostics can be loosely divided into two groups: (A) diagnostics of dust on surfaces and (B) diagnostics of dust in plasma. Group A diagnostics are ultimately more important for next-step devices since they are directly related to monitoring the in-vessel dust inventory. Group B diagnostics should be pursued in contemporary machines since they can provide insight into dust production mechanisms and dust transport. There is also a group of diagnostics that use dust as a tool to diagnose plasmas.[11–13] Since those diagnostics are not designed for dust characterization, they are not discussed in this article.

A. Diagnostics of dust on surfaces

Collection techniques have been used for years to study dust accumulation in fusion devices.[3–5] Samples collected during entry vents allow determination of dust size distribution, chemical composition, and estimation of the in-vessel dust inventory. However, this technique typically provides information averaged over months of operations and thousands of plasma discharges, so correlating dust production and accumulation rates with the discharge parameters is impractical.

Electrostatic detectors[9,14,15] offer a promising new approach to monitoring conductive dust in hard-to-access areas, where dust accumulation is likely to occur in next-step devices (e.g., underneath the divertor dome and targets in ITER). The detector consists of two closely interlocking grids of wires on a circuit board (Fig. 1). To date, prototypes have been fabricated and tested in the laboratory with encouraging results. Tests have also been performed in the NSTX tokamak, but the dust levels proved to be too low for conclusive results. The present sensitivity of the prototype devices is a few tens of ng/cm^2 per count,[15] which is not quite sufficient for contemporary tokamaks, but more than adequate for ITER. An additional benefit of electrostatic detectors is that they eject or evaporate most of the incident dust,[14] and can therefore keep surfaces essentially dust-free.

Capacitive diaphragm microbalance[16,17] is another promising approach for monitoring of dust accumulation in next-step devices. This monitor is based on capacitive manometer technology and is suitable for use in a tokamak environment. A prototype device has been tested in laboratory, where a sensitivity of 500 $\mu g/cm^2$ and dynamic range of at least 10^3 were demonstrated.[17]

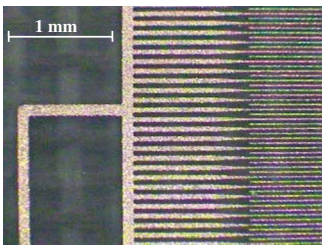

FIG. 1. (Color online) Partial view of circuit grid showing the branching to the finely spaced traces interspersed with the corresponding traces from the right hand side. In the active region, the width of the trace is 25 μm and the trace spacing is 25 μm.

IR thermography[10] can detect the presence of dust on hot PFC surfaces.[18] This may be a valuable tool for checking the compliance with a strict limit for dust on hot surfaces in ITER.

Laser-induced breakdown spectroscopy can be used to locally ablate dust deposited on a surface and determine its chemical composition.[19] However, relating information obtained with this diagnostic to the quantity of the dust on a surface is nontrivial.

Measurements of net erosion of the PFC surfaces allow obtaining an estimate of the upper limit of in-vessel dust inventory[5,16] assuming that all or most of the eroded material is turned into dust. However, for a reasonable estimate multiple locations have to be monitored with sufficient accuracy, and surface dust monitors are still needed to determine where the dust is accumulated.

B. Diagnostics of dust in plasma

Two-dimensional (2D) imaging[2,4,10,12,20–23] allows recording individual particle trajectories and estimating the particle velocities; however, particle size is difficult to determine. Standard frame rate cameras (typically 60 frames/s) generally exhibit a poor contrast ratio for objects moving against the background and can therefore detect only large particles. Fast-framing or gated cameras can resolve smaller, faster moving particles. The use of multiple cameras with intersecting views allows unfolding particle trajectories in full three-dimension (3D).[12,20,23] This capability is invaluable for benchmarking dust dynamics codes such as DUSTT.[7]

Scattering techniques rely on detection of laser light scattered by dust particles within a plasma.[24–26] They allow estimation of size of small particles (comparable to or smaller than the laser wavelength), and measuring dust size distributions and dust density in the plasma. Dust observation rates are generally low, so statistical analysis of the data is required. If the laser beam intensity is high, dust particles can be ablated by the beam, so modeling of the dust-beam interaction is required. Measurements of dust by Mie scattering in DIII-D[25,26] will be discussed in Sec. III.

Spectral survey diagnostics[27,28] generally do not resolve individual dust particles, but can provide an indirect evidence of dust presence in a plasma and elemental information of the dust. Combined survey of impurity lines and thermal continuum radiation is proposed for dust detection (Sec. III).

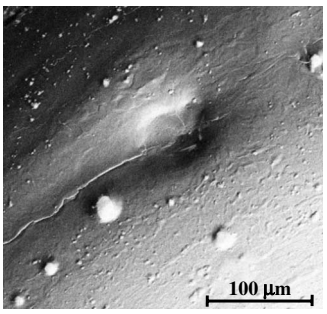

FIG. 2. Crater formed on a surface of a molybdenum probe tip presumably by a hypervelocity dust impact.

Laser-induced incandescence[29,30] is used for dust measurements in processing plasmas. Particle size and possibly concentration can be determined using this technique. Although low dust densities ($\ll 1$ cm^{-3}) in the contemporary tokamak plasmas preclude the use of this technique, it may prove suitable for dust measurements in the far scrape-off layer (SOL) and remote divertor regions of next-step devices.

Langmuir probes[10] can be sensitive to dust provided the dust velocity is sufficiently high. Recent work at FTU tokamak provided evidence of hypervelocity (at or above 10 km/s) particles.[31,32] Signals measured by a probe in the outboard SOL were shown to be consistent with dust particles hitting the probe tip and causing evaporation and ionization of the tip material.[32] Craters observed on the surface of the probe tip upon extraction (Fig. 2) are also consistent with the above picture and difficult to explain otherwise. So far no other machine has reported presence of hypervelocity dust, possibly because no dedicated searches were performed.

Injection of precharacterized dust into plasma[11,21,24] can be used for diagnostic calibration and benchmarking of modeling. Experiments with injected dust in DIII-D are described in Sec. III.

III. DUST MEASUREMENTS IN THE DIII-D TOKAMAK

DIII-D[33] is a tokamak with major and minor radii of 1.67 and 0.67 m, and all-carbon (graphite) PFCs. It has two poloidal divertors and can be operated in lower single null (LSN), upper single null, double null, and wall-limited magnetic configurations. Dust collection has been performed in DIII-D;[3] all other available dust diagnostics belong to group B. Arrangement of the diagnostics used for dust detection in DIII-D is shown in Fig. 3. Shaded areas represent camera views: (1) fast framing camera, (2) tangential divertor TVs, and (3) divertor material evaluation station (DiMES) TV. Dots in (a) show views of spectroscopic diagnostics: (4) multichannel divertor spectrometer (MDS),[27] (5) filterscopes (telescopes with spectral line filters coupled to photomultipliers).[28] MDS lines of view are shown in (b). Outermost viewing volumes of the core (6) and divertor (7) Thomson scattering systems are marked in (b). The location of the DiMES (8) that allows insertion of material samples in the lower divertor[34] is marked in (a) and (b). A poloidal

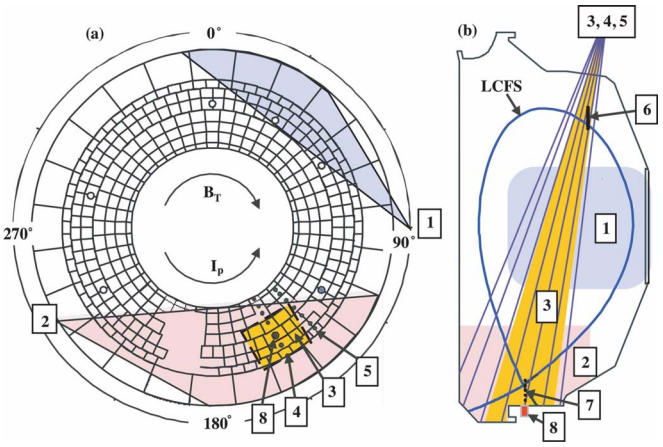

FIG. 3. (Color online) Diagnostic arrangement on DIII-D: (1) fast camera, (2) tangential divertor TVs, (3) DiMES TV, (4) MDS, (5) filterscopes, (6) core Thomson, (7) divertor Thomson, and (8) DiMES.

cross section of a last closed flux surface (LCFS) of a LSN equilibrium with DiMES in the private flux region is shown in (b).

A Thomson scattering system based on eight Nd:YAG lasers is used primarily for the measurements of the electron density and temperature profiles.[35] Each laser produces pulses of about 10 ns duration at a 20 Hz repetition rate with a total energy per pulse of 0.5 J. The vertical core system has four collinear lasers, while the divertor system has a single laser. The laser beam has a center region of high intensity (above 10^{12} W m^{-2}) 3 mm in diameter, surrounded by a halo region with about 5% of the center intensity that extends out to a diameter of 5 mm.[25] Light scattered from multiple positions along the laser path inside the plasma is collected by an optical system located outside the vacuum vessel and directed to polychromators, each with six detectors at different wavelengths. Viewing volumes are typically 1 cm in height and 5 mm in diameter. Nonshifted detector channels at the laser wavelength of 1064 nm allow for detection of light scattered by the dust particles. Signals from large particles cause saturation of the nonshifted channels, but some of them can be resolved by detectors with narrow band filters centered at 1062 nm which have an extinction factor $\sim 10^{-2}$ at the laser wavelength. More detail on dust detection by the Thomson scattering system is available in Ref. 25.

Because of the short laser pulse duration and small viewing volume, dust observation rates are low, only a few events per discharge or less. Nevertheless, statistical analysis of the data provides an estimate of the total dust content in the edge and SOL plasmas, and allows establishing trends in dust production rates. Dust size can be estimated from the amplitude of the scattered signal detected. Initial estimates using the Rayleigh model put resolved size within the range between 50 and 250 nm.[25] However, the Rayleigh approximation is marginal for the larger particles. Another complication in the data interpretation arises from the laser beam energy being sufficient to partially or even completely evaporate smaller particles. A more accurate analysis using a Mie scattering model and taking particle ablation by the laser into account has put the detectable particle size within the range of 0.16–1.6 μm in diameter.[26] Probability distribution func-

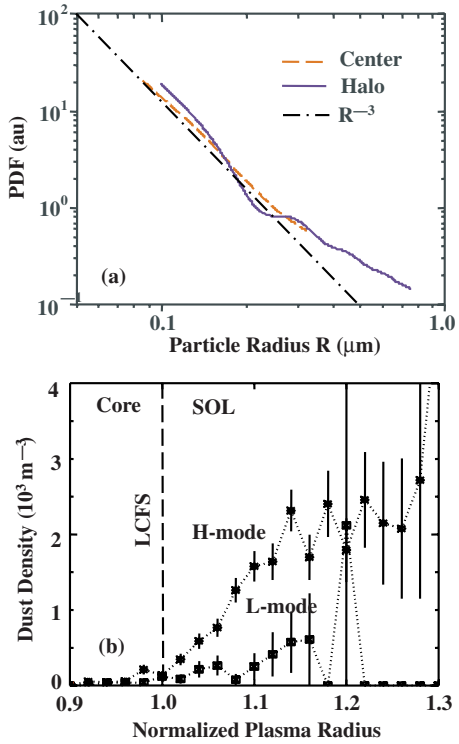

FIG. 4. (Color online) Dust size distribution (a) and radial density profile (b) measured by Mie scattering in DIII-D.

tions (PDFs) of the radii of experimentally detected dust particles are shown in Fig. 4(a). The PDFs were constructed from a fit to the scattering signal distribution obtained over 710 discharges comprising 1580 dust events[25] assuming graphite particles with complex index of refraction $m=3.33-i2.07$.[26] The dashed line is obtained assuming that the detected particles were in the center region of the beam, and the solid line is obtained assuming the particles were in the halo region. For smaller particles ($R<0.2$ μm), the slope of the PDF is close to R^{-3}, while for larger particles it is smaller. Therefore, the contribution of large particles to the total dust mass is larger than that of small ones despite the much larger number density of small particles. Figure 4(b) shows measured dust density profiles in low confinement (L) and high confinement (H) modes. The dust density is near the detection limit at the LCFS and increases with distance into the SOL. It is higher in H mode that has higher heating power and ELMs causing more intense plasma-wall interaction. However, even at the highest dust densities measured and with the dust size determined using the Mie model, the estimated total carbon content of the dust is less than a few percent of the plasma carbon impurity content. Based on this result, submicron dust is not a major impurity source in DIII-D.

Larger dust particles are detected by optical imaging with cameras. A number of standard frame rate complementary metal-oxide semiconductor (CMOS) and charge injection device (CID) cameras and a fast framing CMOS camera are available on DIII-D (Fig. 3). A tangential view of the lower divertor [Fig. 3, view (2)] is split between two standard rate (60 images/s) CID cameras ("tangential TVs"[36]). Spatial resolution of both tangential TVs is about

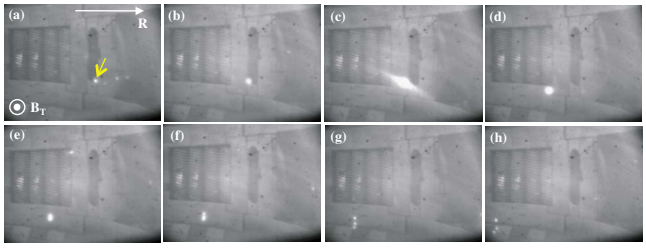

FIG. 5. (Color online) Time history of a dust particle observed by the fast camera in DIII-D SOL. The total time between frames (a) and (h) is ~60 ms, and time between individual frames varies between 8 and 10 ms.

1.5–2.0 cm. A standard rate CMOS camera ("DiMES TV") views vertically down into the lower divertor [Fig. 3, view (3)] with a spatial resolution of about 1.5 mm. A fast framing CMOS camera (Phantom 7.1)[37] has a tangential view of the outboard chamber wall [Fig. 3, view (1)] with a spatial resolution of about 5 mm. The camera has a framing rate of up to 26,000 frames/s at 256×256 pixel resolution. All cameras have remotely changeable filters. Dust particles are occasionally observed with line filters such as D_α, CIII, etc., but most dedicated dust observations are performed either in full light or with Kodak Wratten 89B infrared filters, which block wavelengths below 700 nm. As noted in Sec. II, fast cameras have an inherently higher contrast ratio for moving incandescent objects, and therefore can resolve smaller particles than standard rate cameras. As a result, the dust observation rate using the fast camera is much higher than that of the standard cameras.

During "normal operations," i.e., when the vacuum vessel walls are well conditioned and there are no major disruptions, standard cameras register only isolated dust events in their field of view (typically single digit numbers per discharge or less) while the fast camera typically observes between 10–100 events per discharge. Individual particles move at velocities of up to ~500 m/s. Breakup of larger particles into pieces is sometimes observed. A sequence of frames in Fig. 5 shows a comparatively large and slow (probably tens of microns in size and ~10 m/s in velocity) dust particle marked by an arrow in (a) that first becomes visible in the outboard SOL. Although reconstruction of the exact trajectory from a 2D image is impossible, it appears that the particle first moves toward the LCFS (b), then slows down (c), changes direction (d), and finally breaks into three smaller particles [(e)–(h)]. These data were taken by the fast camera without a filter, at 2000 frames/s with 497 μs exposure per frame. The total time between frames (a) and (h) is ~60 ms, and time between individual frames varies between 8 and 10 ms.

Disruptions often generate significant amounts of dust which is directly observed by the fast framing camera. An image of dust produced by a disruption is shown in Fig. 6(a). A single disruption produces up to ~1000 dust particles within the camera view, corresponding to ~10,000 particles for the whole vessel. Increased dust levels are also observed following entry vents. In the first two to three plasma discharges after an entry vent, standard rate cameras detect hundreds of particles and the fast camera detects thousands of particles in each discharge. An example of dust tracks ob-

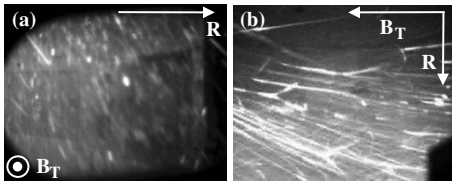

FIG. 6. Dust in DIII-D: (a) dust produced by a disruption (fast camera, tangential view of outboard SOL); (b) dust observed after an entry vent (DiMES TV, looking down in the lower divertor).

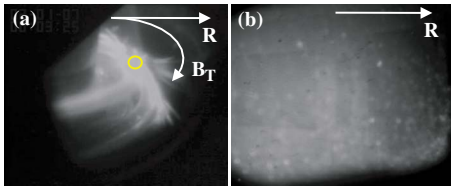

FIG. 7. (Color online) Injected carbon dust in DIII-D observed in divertor by tangential TV (a) and in the SOL by the fast framing camera (b).

served by DiMES TV viewing the lower divertor from above [Fig. 3, view (3)] is shown in Fig. 6(b). After about 15 discharges, dust is virtually gone during the stationary portion of a discharge, and appears at much reduced levels during the plasma initiation and termination phases. After a few days of plasma operations (about 70 discharges) dust levels are further reduced to the normal operations rates.

In principle, if chemical composition and the local plasma parameters at the location of a dust particle are known, one can relate the intensity of thermal radiation from a particle to the particle size.[7,38] If an absolute *in situ* calibration of the camera sensitivity is available, it may be possible to determine the particle size from the intensity of a recorded image, however, in practice this task is extremely complicated. Luminosity of a dust particle is a very strong function of the local plasma density, n_e, and electron temperature, T_e.[7,38] Since gradients of n_e and T_e with typical e-folding lengths of 2–8 cm exist in the SOL,[39] with a 2D view it is practically impossible to determine a particle position with sufficient accuracy for a reasonable size estimate. This complication may be alleviated if multiple cameras with intersecting views are used to determine the particle position in 3D. However, even the accuracy of ± 4 cm achieved in the main chamber SOL of NSTX[20] is at best marginal for a particle size estimate based on its brightness. Moreover, at least in the "near SOL" within a few centimeters of the separatrix, where n_e and T_e are sufficiently high to cause significant ablation of a particle surface, radiation from dust particles observed by cameras is not entirely thermal. Line radiation from the ablation cloud around a particle can contribute significantly to or even dominate the detected radiation. In fact, even though the projection area of a single pixel of a fast camera into DIII-D SOL plasma is ~ 0.2 cm^2, most observed particles appear as multipixel images. The image size most likely reflects the size of the ablation cloud around a particle. This is illustrated in Fig. 5(c) where a large particle clearly develops an ablation cloud appearing as a bright halo elongated along the magnetic field lines.

An alternative approach for determination of a particle size from camera data involves comparison of a particle lifetime in the plasma with a theoretical ablation rate of a carbon sphere.[38] This method has been recently applied in DIII-D. Observed particle sizes between 6 μm and ~ 1 mm and inverse correlation between the particle size and velocity have been inferred.[40]

Injections of precharacterized dust from a known location can be used to calibrate diagnostic measurements and benchmark modeling of dust dynamics and transport. Migration of carbon dust has been studied in DIII-D by introduction of micron-size (0.8–15 μm diameter with a median of ~ 6 μm) graphite dust in the lower divertor.[21] A DiMES sample holder filled with ~ 30 mg of dust was exposed to high-power LSN ELMing *H*-mode discharges with strike points swept across the divertor floor. In the early part of the discharge, the holder with dust was in the private flux region [as shown in Fig. 3(b)], then the outer strike point (OSP) was swept radially inward over the dust. Following a brief exposure (~ 0.1 s) at the OSP, part of the dust was injected into the plasma. A frame from the tangential divertor TV [Fig. 3, view (2)] with IR filter shows a direct view of the injection [Fig. 7(a), the DiMES location is marked by a circle]. About 1.5%–2.0% of the total dust carbon content [$(2-3)\times 10^{19}$ carbon atoms, equivalent to a few million dust particles] penetrated the core plasma, raising the core carbon density by a factor of 2–3 and resulting in a twofold increase in the total radiated power. Individual dust particles were observed moving at velocities of 10–100 m/s, predominantly in the toroidal direction for deuteron flow to the outer divertor target, consistent with the ion drag force. Observed velocities and trajectories of the dust particles are in qualitative agreement with modeling by the DUSTT code,[7,38] which solves equations of motion for dust particles in 3D self-consistently using a plasma background from the UEDGE code. The fast framing camera observed large amounts of injected dust in the outboard SOL [Fig. 7(b)], thus confirming the DUSTT prediction that dust can migrate from the lower divertor into the main chamber.[38] An injection of diamond dust of finely calibrated size between 2 and 4 μm was recently performed. Dust from the injection was observed by the fast camera, but required digital background subtraction to be resolved. Therefore, it was experimentally demonstrated that 4 μm dust is about the smallest that can be resolved by the fast camera in the existing setup at DIII-D.

Filterscopes and MDS spectrometer cannot resolve individual dust particles, but may give indications of dust presence. Figure 8 shows MDS spectra taken at the DiMES location before (lower trace) and after (upper trace) the diamond dust injection. Following the injection, a strong increase in the thermal continuum emission (appearing as a constant offset of the upper trace in Fig. 8) is observed. Concurrent increases in CII emission (5144 mutiplet appearing as three distinct peaks in both traces), C_2 dimer emission (wide band of narrow lines, the so-called Swan band), and CI atomic emission (not shown) were also observed. This observation may be useful for designing novel survey diagnostics for carbon dust in tokamak divertor and SOL plasmas. An increase in the local thermal continuum emission accompanied by increases in atomic and molecular C radiations can

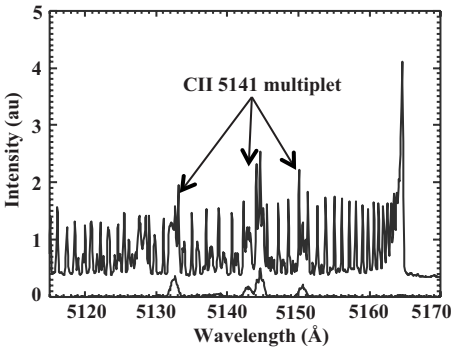

FIG. 8. MDS spectra of CII 5144 multiplet and C_2 dimer Swan band before (lower trace) and after (upper trace) diamond dust injection. Thermal continuum radiation produces the constant base line offset of the upper trace relative to the lower.

be interpreted as a signature of dust presence. An array of optical fibers coupled to detectors with appropriate set of filters can provide a relatively inexpensive way of monitoring dust.

IV. DISCUSSION AND SUMMARY

Dust diagnostics in contemporary tokamaks are still in an early development stage, and considerable progress has yet to be made to meet the challenges in a next-step device such as ITER. However, significant progress has been recently made: prototypes of surface dust diagnostics suitable for use in ITER have been fabricated and tested in laboratory. Various diagnostics of dust in plasmas have been tested in tokamaks with encouraging results, yet there is still considerable space for improvement. For example, scattering diagnostic in DIII-D would benefit from an increased laser beam diameter, eliminating dust ablation by the beam, reducing detector saturation, and increasing the dust observation rate. Intensified fast framing cameras would allow detection of smaller faster particles. Spectral survey diagnostics with appropriate filters may provide a way to monitor dust production rates at multiple locations. Finally, some techniques may be borrowed from other scientific fields; for example, aerogel[41] used by the STARDUST spacecraft to capture comet particles has been proposed for capturing hypervelocity dust particles in a tokamak.

ACKNOWLEDGMENTS

This work was supported in part by the U.S. Department of Energy under DE-FG02-07ER54917, DE-FC02-04ER54698, DE-AC52-07NA27344, DE-AC02-76CH03073, DE-AC04-94AL85000, and DE-FG02-06ER54852.

[1] R. Behrisch, R. S. Blewer, H. Kukral, B. M. U. Scherzer, H. Schmidl, P. Staib, and G. Staudenmaier, J. Nucl. Mater. **76**, 437 (1978).
[2] D. H. J. Goodall, J. Nucl. Mater. **111–112**, 11 (1982).
[3] W. J. Carmack, K. A. McCarthy, D. A. Petti, A. G. Kellman, and C. P. C. Wong, Fusion Eng. Des. **39**, 477 (1998); W. J. Carmack, R. A. Anderl, R. J. Pawelko, G. R. Smolik, and K. A. McCarthy, *ibid.* **51**, 477 (2000).
[4] M. Rubel, M. Cecconelloa, J. A. Malmberga, G. Sergienkob, W. Bielb, J. R. Drakea, A. Hedqvistc, A. Huberb, and V. Philipps, Nucl. Fusion **41**, 1087 (2001).
[5] G. Federici, C. H. Skinner, J. N. Brooks *et al.*, Nucl. Fusion **41**, 1967 (2001).
[6] J. Winter, Plasma Phys. Controlled Fusion **46**, B583 (2004).
[7] A. Yu. Pigarov, S. I. Krasheninnikov, T. K. Soboleva, and T. D. Rognlien, Phys. Plasmas **12**, 122508 (2005).
[8] Z. Wang, C. H. Skinner, G. L. Delzanno, S. I. Krasheninnikov, G. M. Lapenta, A. Yu. Pigarov, P. K. Shukla, *New Aspects of Plasma Physics*, edited by P. K. Shukla, L. Stenflo, and B. Eliasson (World Scientific, Singapore, 2008), pp. 394–475.
[9] C. H. Skinner, A. L. Roquemore, A. Bader, and W. R. Wampler, Rev. Sci. Instrum. **75**, 4213 (2004).
[10] C. J. Lasnier, S. L. Allen, J. A. Boedo, M. Groth, N. H. Brooks, A. McLean, B. LaBombard, C. H. Skinner, D. L. Rudakov, W. P. West, and C. P. C. Wong, Fusion Sci. Technol. **53**, 640 (2008).
[11] Z. Wang and G. A. Wurden, Rev. Sci. Instrum. **74**, 1887 (2003).
[12] Z. Wang, C. M. Ticos, and G. A. Wurden, Phys. Plasmas **14**, 103701 (2007).
[13] Z. Wang and C. M. Ticos, Rev. Sci. Instrum. **79**, 10F333 (2008).
[14] C. V. Parker, C. H. Skinner, and A. L. Roquemore, J. Nucl. Mater. **363–365**, 1461 (2007).
[15] C. H. Skinner, R. Hensley, and A. L. Roquemore, J. Nucl. Mater. **376**, 29 (2008).
[16] G. F. Counsell and C. H. Wu, Phys. Scr., T **T91**, 70 (2001).
[17] G. F. Counsell, A. P. C. de Vere, N. St. J. Braithwaite, S. Hillier, and P. Bjorkman, Rev. Sci. Instrum. **77**, 093501 (2006).
[18] R. Reichle, V. Basiuk, V. Bergeaud, A. Cambe, M. Chantant, E. Delchambre, M. Druetta, E. Gauntier, W. Hess, and C. Pocheau, J. Nucl. Mater. **290–293**, 701 (2001).
[19] G. T. Razdobarin, G. Federici, V. M. Kozhevin, E. E. Mukhin, V. V. Semenov, and S. Yu. Tolstyakov, Fusion Sci. Technol. **41**, 32 (2002).
[20] A. L. Roquemore, N. Nishino, C. H. Skinner, C. Bush, R. Kaita, R. Maqueda, W. Davis, A. Yu Pigarov, and S. I. Krasheninnikov, J. Nucl. Mater. **363–365**, 222 (2007).
[21] D. L. Rudakov, W. P. West, C. P. C. Wong *et al.*, J. Nucl. Mater. **363–365**, 227 (2007).
[22] C. M. Ticos, Z. Wang, G. A. Wurden, J. L. Kline, D. S. Montgomery, L. A. Dorf, and P. K. Shukla, Phys. Rev. Lett. **100**, 155002 (2008).
[23] W. Boeglin, A. L. Roquemore, and R. Maqueda, Rev. Sci. Instrum. **79**, 10F334 (2008).
[24] K. Narihara, K. Toi, Y. Hamada *et al.*, Nucl. Fusion **37**, 1177 (1997).
[25] W. P. West, B. D. Bray, and J. Burkart, Plasma Phys. Controlled Fusion **48**, 1661 (2006).
[26] R. D. Smirnov, W. P. West, S. I. Krasheninnikov, A. Yu. Pigarov, M. Rosenberg, and B. D. Bray, Phys. Plasmas **14**, 112507 (2007).
[27] N. H. Brooks, A. Howald, K. Klepper, and P. West, Rev. Sci. Instrum. **63**, 5167 (1992).
[28] R. J. Colchin, D. L. Hillis, R. Maingi, C. C. Klepper, and N. H. Brooks, Rev. Sci. Instrum. **74**, 2068 (2003).
[29] W. W. Stoffels, E. Stoffels, G. M. W. Kroesen, and F. J. de Hoog, J. Vac. Sci. Technol. A **14**, 588 (1996).
[30] G. S. Eom, C. W. Park, Y. H. Shin, K. H. Chung, S. Park, W. Choe, and J. W. Hahn, Appl. Phys. Lett. **83**, 1261 (2003).
[31] C. Castaldo, S. Ratynskaia, V. Pericoli *et al.*, Nucl. Fusion **47**, L5 (2007).
[32] S. Ratynskaia, C. Castaldo, K. Rypdal, G. Morfill, U. de Angelis, V. Pericoli-Ridolfini, A. Rufoloni, E. Giovannozzi, Nucl. Fusion **48**, 015006 (2008).
[33] J. L. Luxon, Nucl. Fusion **42**, 614 (2002).
[34] C. P. C. Wong, D. G. Whyte, R. J. Bastasz, J. Brooks, W. P. West, and W. R. Wampler, J. Nucl. Mater. **258–263**, 433 (1998).
[35] T. N. Carlstrom, G. L. Campbell, J. C. DeBoo *et al.*, Rev. Sci. Instrum. **63**, 4901 (1992).
[36] M. Groth, M. E. Fenstermacher, C. J. Lasnier, R. Hernandez, J. M. Moller, and R. A. Sturz, Rev. Sci. Instrum. **74**, 2064 (2003).
[37] J. H. Yu, J. A. Boedo, E. M. Hollmann, R. A. Moyer, D. L. Rudakov, and P. B. Snyder, Phys. Plasmas **15**, 032504 (2008).
[38] R. D. Smirnov, A. Yu. Pigarov, M. Rosenberg, S. I. Krasheninnikov, and D. A. Mendis, Plasma Phys. Controlled Fusion **49**, 347 (2007).
[39] D. L. Rudakov, J. A. Boedo, R. A. Moyer *et al.*, Nucl. Fusion **45**, 1589 (2005).
[40] J. H. Yu, D. L. Rudakov, A. Yu. Pigarov, R. D. Smirnov, N. Brooks, S. H. Muller, and W. P. West, "Fast camera imaging of dust in the DIII-D Tokamak," J. Nucl. Mater. (submitted).
[41] See http://stardust.jpl.nasa.gov/photo/aerogel.html for more detail and photographs.